

Gluon helicity distribution in the nucleon from lattice QCD and machine learning

Tanjib Khan,^{1,*} Tianbo Liu,^{2,†} and Raza Sabbir Sufian^{3,‡}

¹*BRAC University, 66 Mohakhali, Dhaka 1212, Bangladesh*

²*Key Laboratory of Particle Physics and Particle Irradiation (MOE), Institute of Frontier and Interdisciplinary Science, Shandong University, Qingdao, Shandong 266237, China*

³*Department of Physics & Astronomy, University of Kentucky, Lexington, KY 40506, US*

We present the first lattice QCD determination of light-cone gluon helicity correlation and parton distribution function (PDF) with numerical evidence toward disfavoring negative gluon polarization in the nucleon. We present a method for eliminating an inevitable contamination term that dominates the Euclidean correlations and makes determining gluon helicity PDF unfeasible. The proposed synergy between lattice QCD and artificial intelligence demonstrates a superior platform to alleviate the defining challenge of extracting quark-gluon PDFs from lattice data that are available in a limited domain due to a finite range of accessible hadron momenta. We suggest a systematically improvable method to extract PDFs from lattice data independent of inadequate parametrizations.

Understanding the internal structure and dynamics of protons and neutrons, the complex many-body systems consisting of strongly interacting quarks and gluons is at the core of exploring the visible matter universe. Specifically, a profound knowledge of the origin of proton's spin is critical for understanding the dynamics of the theory of strong interaction, quantum chromodynamics (QCD). An ongoing effort in theoretical and experimental nuclear physics [1–6], including the future Electron-Ion Collider (EIC) [7–9], is to realize the proton spin decomposition in terms of the quark and gluon spin, and their orbital angular momenta [10, 11] (for reviews, see [12–17]). To explain why the quark spin contributes about 30% to the proton spin, confirmed by analyzing experimental data [18–21] and from recent lattice QCD (LQCD) calculations [22–24], an outstanding problem is to discern how much of the remaining spin budget is from gluons.

In experiments, access to the spin-dependent gluon parton distribution function (PDF) or helicity PDF $\Delta g(x)$ in the nucleon mostly comes from the kinematic region probed by polarized proton-proton collisions at the Relativistic Heavy-Ion Collider (RHIC) in the momentum fraction region, $x \in [0.04, 0.2]$. Excluding the extrapolation of $\Delta g(x)$ in the small- x region, the global analyses [19, 25] obtained sizable positive $\Delta g(x)$ and hence positive gluon polarization ΔG in the nucleon. Depending on whether $\Delta g(x)$ is positive or negative or consistent with zero, the ratio of polarized to unpolarized gluon distribution $\Delta g(x)/g(x)$ can be quite different in the entire x -domain [20]. Two recent analyses [26, 27] found both positive and negative solutions of $\Delta g(x)$ could equally well describe the experimental data. While the future EIC aims to cover presently inaccessible kinematic regions including the unexplored small- x region [28, 29] and provide a stringent constraint on $\Delta g(x)$, it is critically important to determine the nonperturbative $\Delta g(x)$ from first-principles LQCD calculation to provide theoretical support and be complementary to the existing and upcoming experimental programs.

In recent years, several formalisms to determine x -

dependent hadron structures from LQCD have been proposed [30–38]. For reviews of these formalisms and recent lattice calculations see Refs. [39–42]. Among these, the equal-time matrix elements of bilocal operators composed of two gluon fields, known as the quasi-PDF [33] can be used to determine $\Delta g(x)$ using the large momentum effective theory (LaMET) [34]. It has been shown that various combinations of quasi-PDF gluon operators are multiplicatively renormalizable [43, 44], as well as for the case of bilocal quark operators [45–47]. In this work, we use the pseudo-PDF approach [36] based on the quasi-PDF in the Fourier space and a coordinate-space factorization at small distances as proposed in [32]. The pseudo-PDF approach gives only the shape of the gluon helicity Ioffe-time distribution (ITD) [48–50] and a separate calculation of the gluon momentum fraction $\langle x \rangle_g$ is required for proper normalization. However, the multiplicative renormalizability of the quasi-PDF matrix elements utilized for renormalization at short distances using a ratio method [51] is simpler within this approach. In spite of the recent progress in LQCD calculations of the unpolarized gluon PDF [52–57], the determination of $\Delta g(x)$ has not yet been possible due to the presence of a nucleon boost, p_z -dependent contamination term in the off-light-cone matrix elements [58].

In this paper, we propose a solution to this major problem by eliminating the p_z -dependent contamination so that the Euclidean correlation can be matched to the light-cone correlation and be used to extract $\Delta g(x)$. We derive a mathematical relation and implement a machine learning algorithm to perform an extraction of the correlation function that is dominated by the leading-twist contribution. This procedure also has the advantage of alleviating one of the challenging problems to determine gluon PDFs which requires data in a larger range than available from present day LQCD calculations.

To determine $\Delta g(x)$ from LQCD, one needs to calculate matrix elements of gluon field $G_{\mu\nu}$ and its dual $\tilde{G}_{\lambda\beta} = (1/2)\epsilon_{\lambda\beta\rho\gamma}G^{\rho\gamma}$ separated by a spatial Wilson line

$W[z, 0]$ [33, 59]:

$$\Delta M_{\mu\alpha;\lambda\beta}(z, p, s) = \langle p, s | G_{\mu\alpha}(z) W[z, 0] \tilde{G}_{\lambda\beta}(0) | p, s \rangle - (z \rightarrow -z), \quad (1)$$

where z is the separation between the gluon fields, p is the nucleon four-momentum, and s is the nucleon polarization. The combination which gives access to gluon helicity correlation with the least number of contamination terms is $\Delta \mathcal{M}_{00}(z, p_z) \equiv \Delta M_{0i;0i}(z, p_z) + \Delta M_{ij;ij}(z, p_z)$; $i, j = x, y$ being perpendicular to the nucleon boost in the z -direction, $p = \{p_0, 0_\perp, p_z\}$ [59]. Leveraging the multiplicative renormalizability of the link-related UV divergences by forming the following ratio,

$$\Delta \mathfrak{M}(z, p_z) \equiv i \frac{[\Delta \mathcal{M}_{00}(z, p_z)/p_z p_0]/Z_L(z/a_L)}{\mathcal{M}_{00}(z, p_z = 0)/m_p^2}, \quad (2)$$

we obtain the renormalization group invariant reduced pseudo Ioffe-time distribution. Here, $\mathcal{M}_{00}(z, p_z) \equiv [M_{0i;i0}(z, p_z) + M_{ji;ij}(z, p_z)]$ is the spin averaged matrix element related to the unpolarized gluon correlation [54, 60] and the factor $1/Z_L(z/a_L)$ is determined in [59] to cancel the UV logarithmic vertex anomalous dimension of the $\Delta \mathcal{M}_{00}$ matrix element. As a function of Lorentz invariant variables, z^2 and $\omega \equiv z p_z$ (known as the Ioffe time [50] or quasi light-front distance [61]), $\Delta \mathfrak{M}$ can be expressed in terms of invariant amplitudes, $\Delta \mathcal{M}_{sp}^{(+)}$ and $\Delta \mathcal{M}_{pp}$ [59]:

$$\Delta \mathfrak{M}(\omega, z^2) = [\Delta \mathcal{M}_{sp}^{(+)}(\omega, z^2) - \omega \Delta \mathcal{M}_{pp}(\omega, z^2)] - \frac{m_p^2}{p_z^2} \omega \Delta \mathcal{M}_{pp}(\omega, z^2). \quad (3)$$

In contrast, the light-cone correlation that gives access to $x \Delta g(x, \mu)$ at a scale μ is

$$\Delta \mathcal{I}_g(\omega, \mu) \equiv i [\Delta \mathcal{M}_{sp}^{(+)}(\omega, \mu) - \omega \Delta \mathcal{M}_{pp}(\omega, \mu)] = \frac{i}{2} \int_{-1}^1 dx e^{-ix\omega} x \Delta g(x, \mu), \quad (4)$$

and does not contain the additional term $(m_p^2/p_z^2)\omega \Delta \mathcal{M}_{pp}$ as in Eq. (3). A natural choice to suppress this contamination term is to calculate $\Delta \mathfrak{M}(\omega, z^2)$ at a very large momentum. However, even for the nucleon mass, $m_p = 0.938$ GeV and $p_z \approx 3$ GeV, the suppression factor $m_p^2/p_z^2 \approx 0.1$ and the contamination term dominates the matrix elements as ω increases. In addition, achieving good signals for gluonic matrix elements at the physical point and $p_z > 3$ GeV will be very challenging in the near future calculations.

An alternative expression of $\Delta \mathfrak{M}(\omega, z^2)$ shows this matrix element is nonvanishing at $p_z = 0$ [58] and the following subtraction

$$\Delta \mathfrak{M}_{g, \text{sub}}(\omega, z^2) = \Delta \mathcal{M}_{sp}^{(+)}(\omega, z^2) - \omega \Delta \mathcal{M}_{pp}(\omega, z^2) - \omega \frac{m_p^2}{p_z^2} [\Delta \mathcal{M}_{pp}(\omega, z^2) - \Delta \mathcal{M}_{pp}(\omega = 0, z^2)], \quad (5)$$

removes the $\mathcal{O}(\omega)$ contamination but residual higher order contamination can become significant at large ω .

In this work, we propose a method to analytically eliminate the $(m_p^2/p_z^2)\omega \Delta \mathcal{M}_{pp}$ contribution. We take advantage of the fact that different lattice boosts are related by $p_n = 2\pi n/(La)$, where $a = 0.094$ fm is the lattice spacing and $L = 32$ is the spatial extent of the lattice used in this calculation. For simplicity, we omit the subscript z and write $p \equiv p_z$ in the rest of the paper and note that different lattice boosts p_k and p_l are related by the ratio $r = p_k/p_l = k/l$ ($k > l$). Utilizing this relation and multiplying Eq. (3) by corresponding lattice squared-momentum p_k^2 , we get

$$p_k^2 \Delta \mathfrak{M}(\omega)|_{p_k} = p_k^2 [\Delta \mathcal{M}_{sp}^{(+)}(\omega) - \omega \Delta \mathcal{M}_{pp}(\omega)] - m_p^2 \omega \Delta \mathcal{M}_{pp}(\omega), \quad (6)$$

and another set of matrix elements by corresponding p_l^2 , we arrive at the following relation after subtraction:

$$\Delta \mathfrak{M}_g(\omega) \equiv \Delta \mathcal{M}_{sp}^{(+)}(\omega) - \omega \Delta \mathcal{M}_{pp}(\omega) = \frac{r^2 \Delta \mathfrak{M}(\omega)|_{p_k} - \Delta \mathfrak{M}(\omega)|_{p_l}}{r^2 - 1}. \quad (7)$$

Finally, $\Delta \mathfrak{M}_g(\omega)$ is free of the contamination term and can be matched to $\Delta \mathcal{I}_g(\omega, \mu)$. The immediate challenge of implementing Eq. (7) is that the subtractions between multiple p_n data sets require continuous functions in ω and $\Delta \mathfrak{M}$ matrix elements at the same ω . But the LQCD data in FIG. 1 are obtained at discrete ω values and the ranges of ω vary with p_n . In [58], a fit to data using an expansion in moments was performed in an attempt to isolate $[\Delta \mathcal{M}_{sp}^{(+)}(\omega) - \omega \Delta \mathcal{M}_{pp}(\omega)]$ and obtain a continuous distribution in ω among different p_n data sets. An attempt to add only the second moment to parametrize the contamination term containing $\Delta \mathcal{M}_{pp}(\omega)$ resulted in an uncontrolled error and one needed to use the first moment as a Bayesian prior before the error in $\Delta \mathfrak{M}_g(\omega)$ would blow up. Moreover, instead of $i = 0, 1$ in the expression for odd moments $\sum_i \frac{(-1)^i}{(2i+1)!} a_i \omega^{2i+1}$, had it been used $i = 0, 1, 2$, the $\Delta \mathfrak{M}_g(\omega)$ fit in [58] would diverge upward as have been demonstrated in [62, 63]. Therefore, the downward divergent trend of the fitted $\Delta \mathfrak{M}_g(\omega)$ toward negative value completely depends on the truncation of the number of moments and is biased. Similar arguments go for a fit to the noisier $\Delta \mathfrak{M}_{g, \text{sub}}(\omega)$ data using moments.

To solve this problem of parametrization using moments and to determine a contamination-free $\Delta \mathfrak{M}_g(\omega)$, we perform a simultaneous and correlated neural network (NN) analysis to $\Delta \mathfrak{M}(\omega, z^2)$ and $\Delta \mathfrak{M}_{g, \text{sub}}(\omega, z^2)$ data for all values of p_n . The imposed constraint in Eq. (7) serves as the main assumption for the NN. We first parametrize $\Delta \mathfrak{M}$ and $\Delta \mathfrak{M}_{g, \text{sub}}$ into $\Delta \mathcal{I}_g$ plus two different power correction terms in m_p^2/p_n^2 according to Eqs. (3) and (5),

referred to as $C(\omega)$ and $D(\omega)$, respectively. The term $\Delta\mathcal{I}_g(\omega)$ is further parameterized into a prefit function $\Delta\mathcal{I}_{g,0}(\omega)$ multiplied by a deviation function $\delta I(\omega)$. Introducing the prefit function can accelerate the convergence to a smooth function in the fitting, while the result is not sensitive to any particular reasonable choice of $\Delta\mathcal{I}_{g,0}(\omega)$. Here we take a fit curve from Ref. [63].

The architecture of the NN consists of three hidden dense layers with 32, 32, and 8 neurons respectively, activated by the rectified linear unit functions. The first hidden layer is fully connected to the input feature ω . The last hidden layer is fully connected to the output layer, which consists of three neurons corresponding to $\delta I(\omega)$, $C(\omega)$, and $D(\omega)$ up to some shifts and normalization factors, activated by the sigmoid function.

The correlated data sets, $\Delta\mathcal{M}$ and $\Delta\mathcal{M}_{g,\text{sub}}$ are fitted simultaneously with the chi-square as the loss function. For each paired set, 5/6 data from each p -set are randomly selected into the training sample while the remaining 1/6 data are kept for validation. The loss value of the full data set is monitored during the training. It generally decreases at the beginning and starts to increase when overfitting happens, with small fluctuations from epoch to epoch all the time. Eliminating some early epochs to avoid accidental small loss value points, we stop the training when there is no improvement of the total loss value for 3000 epochs and callback the best one.

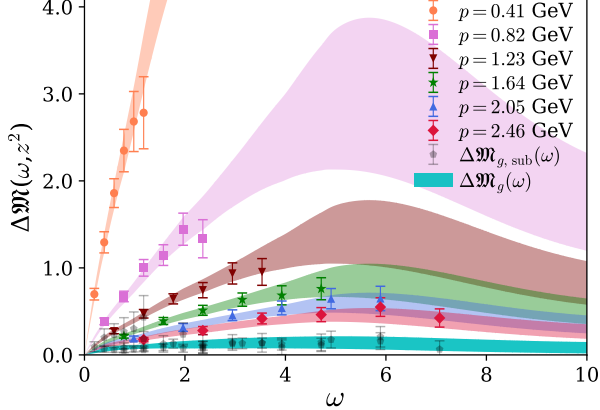


FIG. 1. Neural network fit to $\Delta\mathcal{M}(\omega)$ and $\Delta\mathcal{M}_{g,\text{sub}}(\omega)$ gluonic matrix elements for all p and z_{max} up to $6a$. The cyan band represents the leading-twist dominated $\Delta\mathcal{M}_g(\omega)$.

While a restricted Bayesian fit using only two moments with data up to $\omega = 9.43$ invalidates the fit result for $\omega \gtrsim 4$, the NN uses data up to $\omega \approx 7$ and produces $\Delta\mathcal{M}_g(\omega)$ in an extended region outside the LQCD data. Around $\omega = 11$, the NN extrapolation starts to show oscillation which is expected further outside the lattice data and we consider $\Delta\mathcal{M}_g(\omega)$ up to $\omega_{\text{max}} = 10$ in the subsequent analysis. Quite interestingly, the NN fit does not describe the data well at $z > 6a$. This possibly indicates that $z = 7a, 8a$ data points have significant higher-twist contribution and are not suitable for

extracting the leading-twist dominated $\Delta\mathcal{M}_g(\omega)$ and we limit to $z_{\text{max}} = 6a \approx 0.56$ fm in our analysis. Limiting to $z_{\text{max}} = 5a$ does not change the outcome of the NN analysis much. Although the set in of higher-twist contribution can be observable dependent and data at $z \gtrsim 1$ fm with the assumption of the validity of short-distance factorization has been used in LQCD calculations, e.g. [64], a recent rigorous calculation [65] with implementation of 2-loop matching [66] found that higher-twist contribution can become significant above $z \gtrsim 0.5$ fm (see for other findings [67–69]). With future precise gluonic matrix elements, it remains an open field for investigation up to which z_{max} LQCD data is dominated by the leading-twist contribution and the application of machine learning can be quite useful for this study.

The contamination-free $\Delta\mathcal{M}_g(\omega)$ can now be matched to the light-cone $\Delta\mathcal{I}_g(\omega, \mu)$ and singlet quark ITD $\Delta\mathcal{I}_S(\omega, \mu)$ in the $\overline{\text{MS}}$ scheme using the factorization relation [59] up to power corrections:

$$\begin{aligned} \Delta\mathcal{M}_g(\omega) \langle x \rangle_g(\mu) &= \Delta\mathcal{I}_g(\omega, \mu) - \frac{\alpha_s N_c}{2\pi} \int_0^1 du \Delta\mathcal{I}_g(u\omega, \mu) \\ &\left\{ \ln \left(z^2 \mu^2 \frac{e^{2\gamma_E}}{4} \right) \left(\left[\frac{2u^2}{\bar{u}} + 4u\bar{u} \right]_+ - \left(\frac{1}{2} + \frac{4}{3} \frac{\langle x_S \rangle(\mu)}{\langle x_g \rangle(\mu)} \right) \right. \right. \\ &\delta(\bar{u}) \Big) + 4 \left[\frac{u + \ln(1-u)}{\bar{u}} \right]_+ - \left(\frac{1}{\bar{u}} - \bar{u} \right)_+ - \frac{1}{2} \delta(\bar{u}) \\ &\left. + 2\bar{u}u \right\} - \frac{\alpha_s C_F}{2\pi} \int_0^1 du \Delta\mathcal{I}_S(u\omega, \mu) \left\{ \ln \left(z^2 \mu^2 \frac{e^{2\gamma_E}}{4} \right) \right. \\ &\left. \Delta\mathcal{B}_{gq}(u) + 2\bar{u}u \right\}, \end{aligned} \quad (8)$$

where $N_c = 3$, $\bar{u} \equiv (1-u)$, γ_E is the Euler–Mascheroni constant, $\Delta\mathcal{B}_{gq} = 1 - (1-u)^2$, and we use $\langle x \rangle_g(\mu = 2 \text{ GeV}) = 0.427$ from [23]. Current statistics for gluonic matrix elements does not allow us to observe any logarithmic z^2 -dependence and thus it is not implemented while extracting $\Delta\mathcal{M}_g$. One can subtract $\Delta\mathcal{M}_{pp}$ isolated through the NN analysis from the original LQCD data points and confirm no observed effects. A more sophisticated NN can be implemented to investigate the logarithmic z^2 -dependence with precise matrix elements in future studies. We choose $z = 2a$ and $\mu = 2 \text{ GeV}$ in the matching Eq. (8) and ignore the effect of singlet quark contributions (which requires separate calculations). Taking the singlet distribution from global fit, e.g. NNPDF [70], we find almost no observable impact on the matched $\Delta\mathcal{I}_g$. Similarly, varying values of z or μ has minimal effects on the matched $\Delta\mathcal{I}_g$ within current statistical uncertainty which can be seen from the proximity of $\langle x \rangle_g \Delta\mathcal{M}_g$ and $\Delta\mathcal{I}_g$ bands shown in FIG. 2.

From FIG. 2, it is evident that LQCD calculation of $\Delta\mathcal{I}_g$ disfavors the ITD constructed from negative $x\Delta g(x)$ solution in [26]. Determination of ITDs from negative solution in [26] with varying lower x -limits, for example, $0.01 \leq x \leq 0.99$ or $0.1 \leq x \leq 0.99$ can still be shown

to be ruled out by our calculation in the $\omega \leq 10$ region. This is an important outcome of this LQCD calculation regarding the constraint on the large negative gluon helicity PDF in the moderate to large x -values.

In principle, Gluon helicity in the proton can be obtained from the ITD [50], $\Delta G(\mu) \equiv \int_0^\infty d\omega \Delta \mathcal{I}_g(\omega, \mu)$. On the other hand, integrating $\Delta \mathcal{I}_g(\omega, \mu)$ up to $\omega_{\max} = 10$ from our calculation, we obtain

$$\Delta G^L(\mu) \equiv \int_0^{\omega_{\max}} d\omega \Delta \mathcal{I}_g(\omega, \mu) = 0.405(196). \quad (9)$$

$\Delta G^L(\mu)$ is of course limited by the upper limit of the integration. While $\Delta G^L(\mu)$ in Eq. (9) is a well-defined LQCD measure, the long-tail of the ITD governed by the Regge behavior outside ω_{\max} can lead to underestimation (for a long positive tail) or overestimation (for a negative tail) or some cancellations (for sign change in the tail) of this moment. Example of such an underestimation of the Gegenbauer moment in the pion distribution amplitude calculation can be seen in [71]. One can also try to extrapolate the ITD beyond $\omega_{\max} = 10$ using NN or use phenomenological/model extrapolation of the Regge tail outside the LQCD data [61, 72] and get an estimate of change in ΔG^L . However, the ΔG^L obtained here is expected to depend on the pion mass, lattice spacing, finite volume and on the value of $\langle x \rangle_g$ used from a different lattice ensemble. Since the present work focuses on the methodology and not on the precision study, with these limitations, we refrain from any extrapolation of ΔG^L . On the positive side, a phenomenological analysis [63] found ITD in $\omega \leq 6$ is the mostly affected region for different values of $\Delta G \in [0.2, 0.4]$. Moreover, the only LQCD calculation [73] at the physical pion mass, continuum and infinite volume limits obtained $\Delta G = 0.251(47)(16)$ using a local matrix element [74]. Although the calculation in [73] is not free of a large matching systematic error, it is most likely that the inclusion of various systematics in prospective calculations will not alter the sign of ΔG . It is remarkable that ΔG obtained from this calculation using nonlocal operator and that obtained using a local operator in [73] both result in positive contribution.

Next, we determine $x\Delta g(x, \mu)$ from $\Delta \mathcal{I}_g(\omega, \mu)$. Unlike many previous LQCD calculations (for references see [42]), we avoid constraining the x -dependence of PDF using functional form $x^\alpha(1-x)^\beta$ or an extension to this basic fit form with one or two additional parameters. For currently available LQCD calculations in a limited ω range, these functional forms can be biased, lead to unreliable $\chi^2/\text{d.o.f.}$, and underestimate uncertainties. For example, the same 2-parameter form to parametrize $xg(x)$ led to a diverging PDF in [53] and a converging PDF in [54], whereas none of these lattice ITDs reach anywhere close to the Regge region or have much sensitivity to the small- x physics. This is true for any LQCD calculation in a limited ω range [33, 50]. In [54], $\alpha \geq 0$

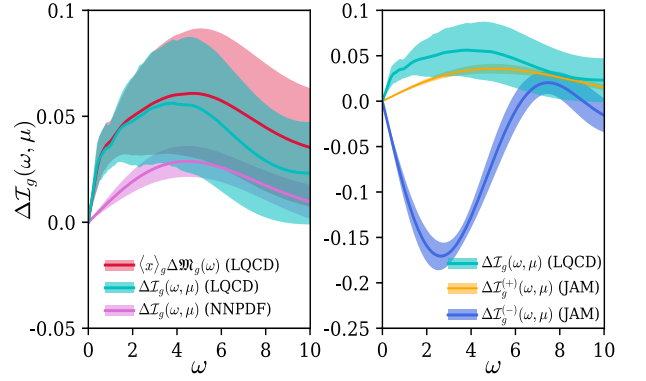


FIG. 2. Comparison of light-cone gluon helicity ITD $\Delta \mathcal{I}_g(\omega, \mu)$ with phenomenological results by the NNPDF [19] (left panel) and JAM [26] (right panel) collaborations. The orange $\Delta \mathcal{I}_g^{(+)}$ and the blue $\Delta \mathcal{I}_g^{(-)}$ bands represent the gluon helicity ITD corresponding to JAM positive and negative $x\Delta g(x)$ solutions, respectively. Pseudo-ITD, $\langle x \rangle_g \Delta \mathcal{M}_g(\omega)$ is shown for comparison by the red band in the left panel figure.

constraint was imposed in a Bayesian fit, motivated by a phenomenological analysis in [63]. Otherwise, it would have resulted in a diverging PDF as in [53]. We, therefore, propose an alternative method to determine $x\Delta g(x)$ from lattice data which is independent of any functional form of PDFs. It can be shown that $x\Delta g(x)$ is related to $\Delta \mathcal{I}_g(\omega, \mu)$ by the following relation:

$$x\Delta g(x, \mu) = \frac{2}{\pi} \int_0^\infty d\omega \sin(x\omega) \Delta \mathcal{I}_g(\omega, \mu), \quad (10)$$

which allows us to obtain $x\Delta g(x, \mu)$ at each point in the x -space as shown in FIG. 3 without relying on any constraint or prior information. Accuracy of the determination of $x\Delta g(x, \mu)$ in this way depends on the available ω_{\max} but gives a true representation of the lattice data and the extracted PDF exactly reproduces the uncertainty of the ITD. It is assuring to see from FIG. 2 that as ω_{\max} increases, $x\Delta g(x, \mu)$ shifts more towards the global analyses results, e.g. the NNPDF and JAM⁽⁺⁾ fits shown in the figure. With increasing ω_{\max} , the accuracy of the determination of PDFs can be systematically improved. It is important to highlight that this calculation does not have a solid constraint on the small- x PDF which is associated with large uncertainties in ΔG and $x\Delta g(x)$ [19, 25] due to lack of experimental data. It is the large negative solution in [26] that exists in the moderate to large x region, is ruled out by our calculation.

In conclusion, we have presented a new methodology of how $x\Delta g(x, \mu)$ can be determined by isolating the leading-twist-dominated component of the gluonic correlation function that could not be achieved previously. We have demonstrated that the interface between LQCD and machine learning can have promising applications to investigate higher-twist contributions at the level of LQCD correlation functions which is an unexplored research area. We have also presented a systematically improvable approach to determine PDF without relying on

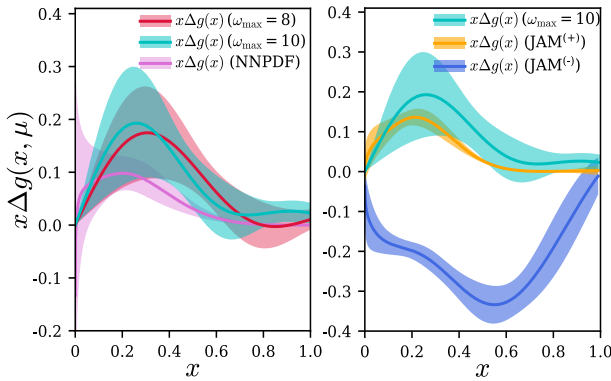


FIG. 3. Functional form independent gluon helicity PDFs (red and cyan bands) from lattice data for two different ranges of ω and comparison with PDFs from NNPDF [19] (left panel) and JAM positive and negative solutions [26] (right panel) at scale $\mu = 2$ GeV.

any restricted functional forms to avoid possible underestimation of uncertainties of the fitted lattice data and PDF. Implementation of these two features will be extended for other quark/gluon correlations in future studies along with application in the LaMET framework to alleviate some of the difficulties in extracting PDFs. Finally, despite the inherent numerical challenges associated with gluonic matrix elements, LQCD calculations will continue to improve significantly, and the calculation of gluon helicity PDF using the proposed methodology can provide essential theoretical support for elucidating the role of gluons in nucleon's spin structure.

Acknowledgement

R.S.S. thanks Nikhil Karthik who provided insight, valuable suggestions, and expertise that greatly assisted this research. R.S.S. acknowledges the mentorship of Robert Edwards, Luka Leskovec, Keh-Fei Liu, Jianwei Qiu, and David Richards and their support and encouragement to pursue this work. We thank members of the HadStruc Collaboration for their interests in our work. T.L. is supported by the National Natural Science Foundation of China under grant Nos. 12175117 and 20221017-1. R.S.S. is supported by the U.S. DOE grant No. DE-SC0013065 and DOE grant No. DE-AC05-06OR23177 which is within the framework of the TMD Topical Collaboration.

* ext.tanjib.atique@bracu.ac.bd

† liutb@sdu.edu.cn

‡ gluon2025@gmail.com

- [1] J. Ashman *et al.* (European Muon Collaboration), *Phys. Lett. B* **206**, 364 (1988).
- [2] J. Ashman *et al.* (European Muon Collaboration), *Nucl. Phys. B* **328**, 1 (1989).

- [3] G. Bunce, N. Saito, J. Soffer, and W. Vogelsang, *Ann. Rev. Nucl. Part. Sci.* **50**, 525 (2000), arXiv:hep-ph/0007218.
- [4] A. Adare *et al.* (PHENIX Collaboration), *Phys. Rev. D* **90**, 012007 (2014), arXiv:1402.6296 [hep-ex].
- [5] A. Airapetian *et al.* (HERMES Collaboration), *JHEP* **06**, 066 (2008), arXiv:0802.2499 [hep-ex].
- [6] R. Akhunzyanov *et al.* (COMPASS Collaboration), *Phys. Lett. B* **793**, 188 (2019), [Erratum: *Phys. Lett. B* **800**, 135129 (2020)], arXiv:1802.02739 [hep-ex].
- [7] A. Accardi *et al.*, *Eur. Phys. J. A* **52**, 268 (2016), arXiv:1212.1701 [nucl-ex].
- [8] R. Abdul Khalek *et al.*, *Nucl. Phys. A* **1026**, 122447 (2022), arXiv:2103.05419 [physics.ins-det].
- [9] D. P. Anderle *et al.*, *Front. Phys. (Beijing)* **16**, 64701 (2021), arXiv:2102.09222 [nucl-ex].
- [10] R. L. Jaffe and A. Manohar, *Nucl. Phys. B* **337**, 509 (1990).
- [11] X.-D. Ji, *Phys. Rev. Lett.* **78**, 610 (1997), arXiv:hep-ph/9603249.
- [12] C. A. Aidala, S. D. Bass, D. Hasch, and G. K. Mallot, *Rev. Mod. Phys.* **85**, 655 (2013), arXiv:1209.2803 [hep-ph].
- [13] E. Leader and C. Lorcé, *Phys. Rep.* **541**, 163 (2014), arXiv:1309.4235 [hep-ph].
- [14] M. Wakamatsu, *Int. J. Mod. Phys. A* **29**, 1430012 (2014), arXiv:1402.4193 [hep-ph].
- [15] A. Deur, S. J. Brodsky, and G. F. de Tera mond, *Rep. Prog. Phys.* **82**, 076201 (2018), arXiv:1807.05250 [hep-ph].
- [16] X. Ji, F. Yuan, and Y. Zhao, *Nature Rev. Phys.* **3**, 27 (2021), arXiv:2009.01291 [hep-ph].
- [17] K.-F. Liu, *AAPPS Bull.* **32**, 8 (2022), arXiv:2112.08416 [hep-lat].
- [18] D. de Florian, R. Sassot, M. Stratmann, and W. Vogelsang, *Phys. Rev. D* **80**, 034030 (2009), arXiv:0904.3821 [hep-ph].
- [19] E. R. Nocera, R. D. Ball, S. Forte, G. Ridolfi, and J. Rojo (NNPDF Collaboration), *Nucl. Phys. B* **887**, 276 (2014), arXiv:1406.5539 [hep-ph].
- [20] C. Adolph *et al.* (COMPASS Collaboration), *Phys. Lett. B* **753**, 18 (2016), arXiv:1503.08935 [hep-ex].
- [21] J. J. Ethier, N. Sato, and W. Melnitchouk, *Phys. Rev. Lett.* **119**, 132001 (2017), arXiv:1705.05889 [hep-ph].
- [22] H.-W. Lin, R. Gupta, B. Yoon, Y.-C. Jang, and T. Bhattacharya, *Phys. Rev. D* **98**, 094512 (2018), arXiv:1806.10604 [hep-lat].
- [23] C. Alexandrou, S. Bacchio, M. Constantinou, J. Finkenrath, K. Hadjiyiannakou, K. Jansen, G. Koutsou, H. Panagopoulos, and G. Spanoudes, *Phys. Rev. D* **101**, 094513 (2020), arXiv:2003.08486 [hep-lat].
- [24] G. Wang, Y.-B. Yang, J. Liang, T. Draper, and K.-F. Liu (χ QCD), *Phys. Rev. D* **106**, 014512 (2022), arXiv:2111.09329 [hep-lat].
- [25] D. de Florian, R. Sassot, M. Stratmann, and W. Vogelsang, *Phys. Rev. Lett.* **113**, 012001 (2014), arXiv:1404.4293 [hep-ph].
- [26] Y. Zhou, N. Sato, and W. Melnitchouk, *Phys. Rev. D* **105**, 074022 (2022), arXiv:2201.02075 [hep-ph].
- [27] R. M. Whitehill, Y. Zhou, N. Sato, and W. Melnitchouk, (2022), arXiv:2210.12295 [hep-ph].
- [28] E. C. Aschenauer, R. Sassot, and M. Stratmann, *Phys. Rev. D* **92**, 094030 (2015), arXiv:1509.06489 [hep-ph].

- [29] I. Borsa, G. Lucero, R. Sassot, E. C. Aschenauer, and A. S. Nunes, *Phys. Rev. D* **102**, 094018 (2020), [arXiv:2007.08300 \[hep-ph\]](#).
- [30] K.-F. Liu and S.-J. Dong, *Phys. Rev. Lett.* **72**, 1790 (1994), [arXiv:hep-ph/9306299](#).
- [31] W. Detmold and C. J. D. Lin, *Phys. Rev. D* **73**, 014501 (2006), [arXiv:hep-lat/0507007](#).
- [32] V. Braun and D. Müller, *Eur. Phys. J. C* **55**, 349 (2008), [arXiv:0709.1348 \[hep-ph\]](#).
- [33] X. Ji, *Phys. Rev. Lett.* **110**, 262002 (2013), [arXiv:1305.1539 \[hep-ph\]](#).
- [34] X. Ji, *Sci. China Phys. Mech. Astron.* **57**, 1407 (2014), [arXiv:1404.6680 \[hep-ph\]](#).
- [35] A. J. Chambers, R. Horsley, Y. Nakamura, H. Perlt, P. E. L. Rakow, G. Schierholz, A. Schiller, K. Somfleth, R. D. Young, and J. M. Zanotti, *Phys. Rev. Lett.* **118**, 242001 (2017), [arXiv:1703.01153 \[hep-lat\]](#).
- [36] A. V. Radyushkin, *Phys. Rev. D* **96**, 034025 (2017), [arXiv:1705.01488 \[hep-ph\]](#).
- [37] Y.-Q. Ma and J.-W. Qiu, *Phys. Rev. D* **98**, 074021 (2018), [arXiv:1404.6860 \[hep-ph\]](#).
- [38] Y.-Q. Ma and J.-W. Qiu, *Phys. Rev. Lett.* **120**, 022003 (2018), [arXiv:1709.03018 \[hep-ph\]](#).
- [39] K. Cichy and M. Constantinou, *Adv. High Energy Phys.* **2019**, 3036904 (2019), [arXiv:1811.07248 \[hep-lat\]](#).
- [40] M. Constantinou *et al.*, *Prog. Part. Nucl. Phys.* **121**, 103908 (2021), [arXiv:2006.08636 \[hep-ph\]](#).
- [41] X. Ji, Y.-S. Liu, Y. Liu, J.-H. Zhang, and Y. Zhao, *Rev. Mod. Phys.* **93**, 035005 (2021), [arXiv:2004.03543 \[hep-ph\]](#).
- [42] M. Constantinou *et al.*, (2022), [arXiv:2202.07193 \[hep-lat\]](#).
- [43] J.-H. Zhang, X. Ji, A. Schäfer, W. Wang, and S. Zhao, *Phys. Rev. Lett.* **122**, 142001 (2019), [arXiv:1808.10824 \[hep-ph\]](#).
- [44] Z.-Y. Li, Y.-Q. Ma, and J.-W. Qiu, *Phys. Rev. Lett.* **122**, 062002 (2019), [arXiv:1809.01836 \[hep-ph\]](#).
- [45] T. Izubuchi, X. Ji, L. Jin, I. W. Stewart, and Y. Zhao, *Phys. Rev. D* **98**, 056004 (2018), [arXiv:1801.03917 \[hep-ph\]](#).
- [46] X. Ji, J.-H. Zhang, and Y. Zhao, *Phys. Rev. Lett.* **120**, 112001 (2018), [arXiv:1706.08962 \[hep-ph\]](#).
- [47] J. Green, K. Jansen, and F. Steffens, *Phys. Rev. Lett.* **121**, 022004 (2018), [arXiv:1707.07152 \[hep-lat\]](#).
- [48] V. N. Gribov, B. L. Ioffe, and I. Y. Pomeranchuk, *Yad. Fiz.* **2**, 768 (1965).
- [49] B. L. Ioffe, *Phys. Lett. B* **30**, 123 (1969).
- [50] V. Braun, P. Gornicki, and L. Mankiewicz, *Phys. Rev. D* **51**, 6036 (1995), [arXiv:hep-ph/9410318](#).
- [51] K. Orginos, A. Radyushkin, J. Karpie, and S. Zafeiropoulos, *Phys. Rev. D* **96**, 094503 (2017), [arXiv:1706.05373 \[hep-ph\]](#).
- [52] Z.-Y. Fan, Y.-B. Yang, A. Anthony, H.-W. Lin, and K.-F. Liu, *Phys. Rev. Lett.* **121**, 242001 (2018), [arXiv:1808.02077 \[hep-lat\]](#).
- [53] Z. Fan, R. Zhang, and H.-W. Lin, *Int. J. Mod. Phys. A* **36**, 2150080 (2021), [arXiv:2007.16113 \[hep-lat\]](#).
- [54] T. Khan *et al.* (HadStruc Collaboration), *Phys. Rev. D* **104**, 094516 (2021), [arXiv:2107.08960 \[hep-lat\]](#).
- [55] Z. Fan and H.-W. Lin, *Phys. Lett. B* **823**, 136778 (2021), [arXiv:2104.06372 \[hep-lat\]](#).
- [56] A. Salas-Chavira, Z. Fan, and H.-W. Lin, (2021), [arXiv:2112.03124 \[hep-lat\]](#).
- [57] Z. Fan, W. Good, and H.-W. Lin, (2022), [arXiv:2210.09985 \[hep-lat\]](#).
- [58] C. Egerer *et al.* (HadStruc), *Phys. Rev. D* **106**, 094511 (2022), [arXiv:2207.08733 \[hep-lat\]](#).
- [59] I. Balitsky, W. Morris, and A. Radyushkin, *JHEP* **02**, 193 (2022), [arXiv:2112.02011 \[hep-ph\]](#).
- [60] I. Balitsky, W. Morris, and A. Radyushkin, *Phys. Lett. B* **808**, 135621 (2020), [arXiv:1910.13963 \[hep-ph\]](#).
- [61] X. Ji, Y. Liu, A. Schäfer, W. Wang, Y.-B. Yang, J.-H. Zhang, and Y. Zhao, *Nucl. Phys. B* **964**, 115311 (2021), [arXiv:2008.03886 \[hep-ph\]](#).
- [62] A. Saalfeld, G. Piller, and L. Mankiewicz, *Eur. Phys. J. C* **4**, 307 (1998), [arXiv:hep-ph/9708378](#).
- [63] R. S. Sufian, T. Liu, and A. Paul, *Phys. Rev. D* **103**, 036007 (2021), [arXiv:2012.01532 \[hep-ph\]](#).
- [64] C. Egerer, R. G. Edwards, C. Kallidonis, K. Orginos, A. V. Radyushkin, D. G. Richards, E. Romero, and S. Zafeiropoulos (HadStruc Collaboration), *JHEP* **11**, 148 (2021), [arXiv:2107.05199 \[hep-lat\]](#).
- [65] M. Bhat, W. Chomicki, K. Cichy, M. Constantinou, J. R. Green, and A. Scapellato, *Phys. Rev. D* **106**, 054504 (2022), [arXiv:2205.07585 \[hep-lat\]](#).
- [66] Z.-Y. Li, Y.-Q. Ma, and J.-W. Qiu, *Phys. Rev. Lett.* **126**, 072001 (2021), [arXiv:2006.12370 \[hep-ph\]](#).
- [67] N. Karthik and R. S. Sufian, *Phys. Rev. D* **104**, 074506 (2021), [arXiv:2106.03875 \[hep-lat\]](#).
- [68] X. Ji, (2022), [arXiv:2209.09332 \[hep-lat\]](#).
- [69] Y. Su, J. Holligan, X. Ji, F. Yao, J.-H. Zhang, and R. Zhang, (2022), [arXiv:2209.01236 \[hep-ph\]](#).
- [70] R. D. Ball *et al.* (NNPDF Collaboration), *Eur. Phys. J. C* **77**, 663 (2017), [arXiv:1706.00428 \[hep-ph\]](#).
- [71] X. Gao, A. D. Hanlon, N. Karthik, S. Mukherjee, P. Petreczky, P. Scior, S. Syritsyn, and Y. Zhao, *Phys. Rev. D* **106**, 074505 (2022), [arXiv:2206.04084 \[hep-lat\]](#).
- [72] X. Gao, A. D. Hanlon, S. Mukherjee, P. Petreczky, P. Scior, S. Syritsyn, and Y. Zhao, *Phys. Rev. Lett.* **128**, 142003 (2022), [arXiv:2112.02208 \[hep-lat\]](#).
- [73] Y.-B. Yang, R. S. Sufian, A. Alexandru, T. Draper, M. J. Glatzmaier, K.-F. Liu, and Y. Zhao, *Phys. Rev. Lett.* **118**, 102001 (2017), [arXiv:1609.05937 \[hep-ph\]](#).
- [74] X. Ji, J.-H. Zhang, and Y. Zhao, *Phys. Rev. Lett.* **111**, 112002 (2013), [arXiv:1304.6708 \[hep-ph\]](#).